Broadband behavior of quadratic metalenses with a wide field of view

Yang Liu, Jianhao Zhang, Xavier Le Roux, Eric Cassan, Delphine Marris-Morini, Laurent Vivien, Carlos Alonso-Ramos, Daniele Melati

Research Article | Vol. 30, No. 22 / 24 Oct 2022 / Optics Express 39860
Optics EXPRESS

Broadband behavior of quadratic metalenses with a wide field of view

YANG LIU,[1,2] JIANHAO ZHANG,[1] XAVIER LE ROUX,[1] ERIC CASSAN,[1] DELPHINE MARRIS-MORINI,[1] LAURENT VIVIEN,[1] CARLOS ALONSO-RAMOS,[1] AND DANIELE MELATI[1,*]

[1] *Centre de Nanosciences et de Nanotechnologies, Université Paris-Saclay, CNRS, 91120 Palaiseau, France*
[2] *Currently with DTU Fotonik, Technical University of Denmark, (Ø)rsteds Plads 343, 2800 Kgs. Lyngby, Denmark*
[*] *daniele.melati@universite-paris-saclay.fr*

Abstract: Metalenses are attracting a large interest for the implementation of complex optical functionalities in planar and compact devices. However, chromatic and off-axis aberrations remain standing challenges. Here, we experimentally investigate the broadband behavior of metalenses based on quadratic phase profiles. We show that these metalenses do not only guarantee an arbitrarily large field of view but are also inherently tolerant to longitudinal and transverse chromatic aberrations. As such, we demonstrate a single-layer, silicon metalens with a field of view of 86° and a bandwidth up to 140 nm operating at both 1300 nm and 1550 nm telecommunication wavelength bands.

1. Introduction

Metasurfaces are two-dimensional arrangements of subwavelength scattering elements capable of manipulating the phase, amplitude, and polarization of a wave front [1,2]. This technology has been successfully exploited to realize compact and flat planar devices implementing a variety of optical functionalities, including lenses, holograms, mirrors, and polarizers, to name a few [3–5]. The possibility to precisely tailor the optical response of each element in the metasurface (meta-atom) provides an invaluable design freedom. This notoriously enabled, among other examples, the demonstration of high-performance metalenses free of spherical aberration for on-axis propagation reaching diffraction-limited resolution at a specific wavelength [6,7]. However, despite great findings, simultaneously ensuring broadband operation and wide field of view still remains challenging for metalenses [8–10], an aspect of fundamental importance in many applications including imaging and beam steering. A number of designs with compensation of chromatic aberration have been proposed, mostly relying on the judicious engineering of meta-atoms dispersion [11–15], but commonly restricted to on-axis propagation or small incidence angles. Likewise, metalenses with a large field of view have been obtained using cascaded, multi-layer structures (doublets) [16,17] and aperture stops [18], but limited to monochromatic operation or moderate bandwidths [19]. Very recently, achromatic metalenses demonstrating also a wide field of view have been achieved using optimized phase profiles designed via deep learning techniques [20] and exploiting metalens doublets [21].

Interestingly, it has also been shown that it is possible to realize a metalens with a full 180° field of view by trading-off the diffraction-limited resolution offered by the common hyperbolic phase profile and exploiting instead a quadratic phase profile [22–25]. While hyperbolic profiles achieve excellent focusing performance and have been largely explored for the design of achromatic metalenses, their behavior quickly degrades with off-axis illumination, resulting in a narrow field of view. On the contrary, quadratic phase profiles provide a point spread function that remains undistorted upon tilted illumination and can hence represent a good candidate for the realization of metalenses that simultaneously have a large field of view and wavelength-tolerant performance.

#466321 https://doi.org/10.1364/OE.466321
Journal © 2022 Received 9 Jun 2022; revised 19 Aug 2022; accepted 30 Aug 2022; published 13 Oct 2022

Optics EXPRESS

While the single-wavelength performance of such quadratic metalenses has been described in details, to our knowledge their broadband behavior has not yet been extensively studied, limiting their potential applicability in multi-wavelength systems. Only an initial qualitative demonstration of a rather large tolerance to longitudinal chromatic aberration has been reported in [22].

In this work, we experimentally investigate, for the first time, the behavior of a single-layer metalens with a wide field of view based on a quadratic phase profile over two broad wavelength ranges at typical telecommunication wavelengths of 1300 nm and 1550 nm. Even if the metalens is not designed to be achromatic, we show that, due to the large depth of focus, the size of the lens focal spot remains unchanged across both wavelength bands, quantitatively confirming the tolerance to longitudinal chromatic aberration. Furthermore, we also demonstrate that the reduced resolution of quadratic metalenses helps in achieving a large tolerance to transverse chromatic aberration, an aspect that has not been addressed before but of central importance for metalenses with a wide field of view. The metalens was realized on a silicon platform with a nominal numerical aperture of 0.83 and, overall, we simultaneously show a measured spectral bandwidth of 140 nm and a wide field of view of 86°, limited only by our experimental setup.

2. Quadratic metalens design

The phase delay imparted by a quadratic metalens to an incoming wavefront is described by

$$\varphi(r) = -\frac{\omega n_{\mathrm{f}}}{2cf} r^2. \tag{1}$$

In Eq. (1), ω is the frequency of the light, n_{f} is the refractive index of the material where light is focused, c is the speed of light, f is the focal distance of the metalens, and r is the radial distance from the center of the lens. As schematically illustrated in Fig. 1(a), assuming the metalens lies in the xy plane and a plane wave arrives with an incident angle θ from the normal in the xz plane, propagating in a medium with refractive index n_{c}, the phase front after the metalens becomes

$$\varphi(r) = -\frac{\omega n_{\mathrm{f}}}{2cf} r^2 - \frac{\omega}{c} n_{\mathrm{c}} x \sin\theta = -\frac{\omega n_{\mathrm{f}}}{2cf}\left[\left(x + \frac{n_{\mathrm{c}}}{n_{\mathrm{f}}} f \sin\theta\right)^2 + y^2\right] + \frac{\omega f n_{\mathrm{c}}^2 \sin^2\theta}{2c n_{\mathrm{f}}} \tag{2}$$

The second term in Eq. (2) does not depend on the radial distance and can be neglected since it does not influence the shape of the wavefront. Comparing the first term of Eq. (2) with Eq. (1), it can be seen that the oblique incidence results in a transverse shift of the focal spot in the x direction:

$$\Delta x = \frac{n_{\mathrm{c}}}{n_{\mathrm{f}}} f \sin\theta \tag{3}$$

The use of a quadratic phase profile hence allows to achieve a full 180° field of view by focusing light beams incident at different angles on a planar image plane with an undistorted focal spot. However, a quadratic phase profile also introduces spherical aberration and a large depth of focus [22]. This results in a reduced resolution compared for example to diffraction-limited metalenses based on hyperbolic phase profiles, as thoroughly discussed in [24].

In order to implement the described phase profile, we use 700-nm-high silicon meta-atoms on SiO_2, as shown in Fig. 1(a,b). The design is done at λ = 1550 nm using for silicon the refractive index n_{Si} = 3.47. Since focusing occurs in air and illumination is made through the SiO_2 substrate, we consider n_{f} = 1 and n_{c} = 1.444. A fishnet structure is chosen to ensure a better mechanical stability of the meta-atoms. The metalens is realized with a lattice period of 800 nm that avoids high-order diffraction in the far field, provides a sufficiently accurate sampling of the phase profile, and enables a large feature size to ensure a reliable fabrication. To design the metasurface, the dimensions L_1 and L_2 of the rectangular pillars are varied between 200 nm and 700 nm. The cross width is fixed at 100 nm. For each combination of L_1 and L_2, we

Optics EXPRESS

compute the phase and transmission of the meta-atom by simulating a corresponding periodic array for normal incidence through the Rigorous Coupled Wave Analysis [26]. We then disregard all meta-atoms with transmission efficiency lower than 0.5 to reduce the metalens losses and spurious amplitude modulations. Simulation results at $\lambda = 1550$ nm are reported in Fig. 1(c,d), respectively. The remaining library of meta-atoms allows to cover the entire phase range between $-\pi$ and π and is eventually used to discretize the phase profile (1) by properly organizing the meta-atoms according to the required phase $\varphi(r)$. In case of meta-atoms with equivalent phase delay, we select the one with the highest transmission efficiency. It should be noted that, under oblique incidence, the transmission efficiency of the meta-atoms tends to reduce (see Fig. S1 of Supplement 1), introducing additional losses for the metalens. These losses could be mitigated exploiting different types of meta-atoms, for example substituting the fishnet structure with simpler silicon pillars.

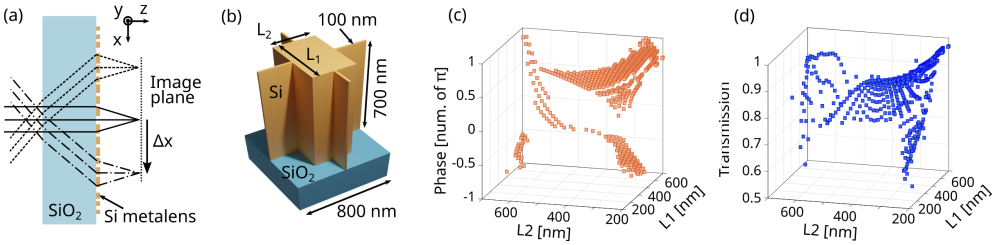

Fig. 1. Design of the quadratic metalens. (a) Schematic diagram of the metalens operation. The shape of the focal spot does not change with oblique incidence but only shift on the image plane. (b) Schematic of the meta-atom used to realize the fishnet metalens. The two dimensions of the silicon pillars L_1 and L_2 are independently chosen. (c) Phase and (d) amplitude response of the meta-atoms as a function of L_1 and L_2.

3. Broadband behavior of the metalens

We fabricated a metalens with a diameter D = 240 μm and a focal length in air $f = 80$ μm at a wavelength $\lambda = 1550$ nm, resulting in a high nominal numerical aperture NA = 0.83 (the phase profile of the metalens is shown in Fig. S2 of Supplement 1). As detailed below, a numerical aperture larger than 0.8 is necessary for the metalens to achieve an arbitrarily large field of view. The fabrication was done using electron beam lithography and dry etching. Scanning electron microscope pictures of the realized device are shown in Fig. 2 and in Fig. S3 of Supplement 1. The collimated output of a tunable laser with a waist diameter of 3.6 mm was used to illuminate the metalens at different angles and light wavelengths. The corresponding point spread function was then imaged on an InGaAs camera through a 40X objective with numerical aperture of 0.65 and a tube lens with focal distance of 200 mm. The metalens was mounted on a piezoelectric translation stage to allow imaging of the three-dimensional intensity distribution of light after the metalens. A schematic representation of the experimental setup is shown in Fig. S4 of Supplement 1.

The measured intensity distributions in the horizontal axial plane (xz cross section, see Fig. 1(a) for the reference axes) are plotted in Fig. 3(a) for wavelength ranging from 1500 nm to 1640 nm and illumination angles from 0° to 43°. Our setup did not allowed to further increase the illumination angle. The origin of the z axis is arbitrary but fixed throughout the measurements. The corresponding image plane intensities (transverse xy plane) are shown in Fig. 3(b). All focal spots are imaged at a distance of 55 μm from the origin along the z axis, as marked by the white dashed lines in Fig. 3(a). While longitudinal chromatic aberration causes the focal distance to reduce at longer wavelengths, the relative large depth of focus allows overcoming the

Optics EXPRESS

effect of the shift and enables the metalens to operate at a constant image plane within a broad bandwidth. An almost unchanged focal spot is maintained across the entire wavelength range and also at different illumination angles. At tilted illumination, the position of the focal spot on the image plane simply laterally shifts along the x direction, as described by Eq. (3). To further investigate the broadband behavior of the metalens, we repeated the measurement of the point spread function for a wavelength range centered around λ = 1300 nm. Results are reported in Fig. 4 for normal and tilted illumination at 23° and 43°. Measurement cuts along both the axial xz plane and the image xy plane are reported. Due to chromatic aberration, the image plane moved to z = 72 µm, a distance of about 17 µm along the z direction compared to the images of Fig. 3(b). Despite being designed to operate at λ = 1550 nm, a large and broadband field of view could be obtained also in this case, with well defined and undistorted focal spots for the different illumination angles and wavelengths between 1260 nm and 1340 nm. Fig. 5 presents a more detailed analysis of the performance of the metalens. In particular, we quantified the effect of longitudinal and transverse chromatic aberration which cause the focal spot to move along the z and x axes, respectively, when wavelength is varied. While for lenses with a small field of view transverse chromatic aberration can often be overlooked, it becomes here a relevant parameter to define the off-axis behavior of the lens [20]. The measured displacement Δx along the x axis as a function of the illumination angle is shown in Fig. 5(a) for sampled wavelengths across both the 1500 nm - 1640 nm (blue squares) and 1260 nm - 1340 nm ranges (orange dots). As already mentioned, the 43° limit is due to our measurement setup and not to the metalens design. Full ±90° field of view has already been demonstrated using quadratic metalenses [24]. The displacement is perfectly fit by Eq. (3) using a focal length f = 79 µm at λ = 1550 nm (as expected from the design) and f = 96 µm at λ = 1300 nm.

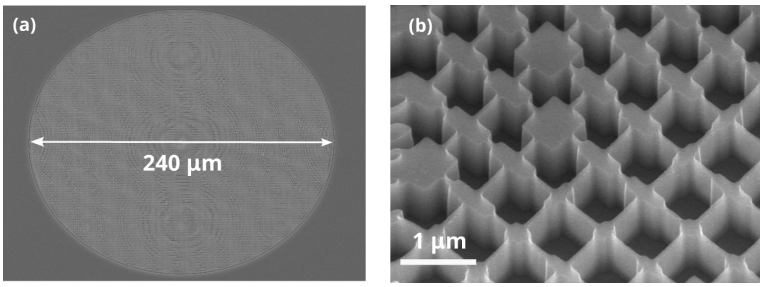

Fig. 2. Scanning electron microscope (SEM) pictures of the fabricated quadratic metalens. (a) Full device and (b) close-up on a few lattice periods showing the quality of the fabricated device.

From the displacement measurements it is possible to estimate the effect of the longitudinal chromatic aberration within the two considered wavelength ranges. The maximum longitudinal chromatic shift from the mean focal length along the z axis is limited to 4 µm for the 1550 nm range (5% relative focal shift over a 140-nm bandwidth) and 3 µm for the 1300 nm range (3% relative focal shift over a 100-nm bandwidth). This confirms that the relatively small chromatic focal shifts combined with the large depth of focus enables the fixed image plane to fall within the focal tolerance of the lens throughout both spectral ranges, as previously shown in Figs. 3 and 4. Regarding transverse chromatic aberration, the deviation of the displacement Δx of the spot on the image plane caused by a variation of the wavelength for θ = 43° is about 3 µm and 2 µm in the measured ranges around λ = 1550 nm and λ = 1300 nm, respectively. This wavelength-dependent transverse shift becomes more pronounced as the illumination angle grows. However, at θ = 90° the maximum longitudinal focal shift also corresponds to the maximum deviation of the transverse displacement Δx, which is hence limited to 4 µm and 3 µm in the

Optics EXPRESS

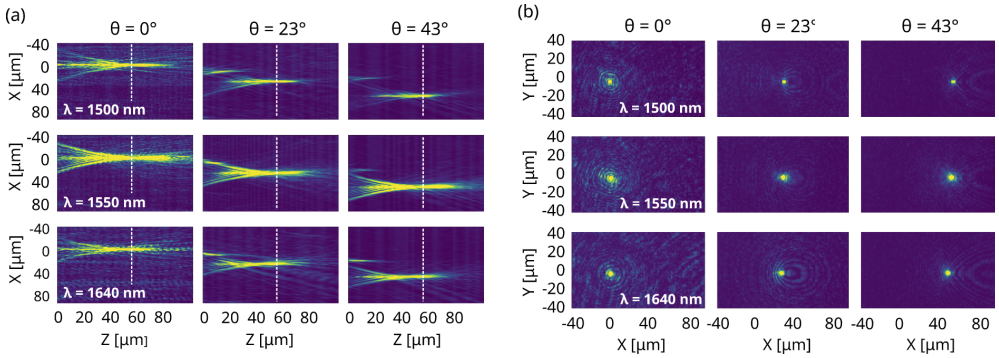

Fig. 3. Experimental results of broadband and wide-angle focusing. (a) Measured intensity profiles in the axial xz plane, being z the propagation direction, at different wavelengths from 1500 nm to 1640 nm and illuminating angles from 0° to 43°. (b) Intensity profiles at the image plane marked by the dashed lines in (a) (z = 55 μm, transverse xy plane) for the same wavelengths and angles.

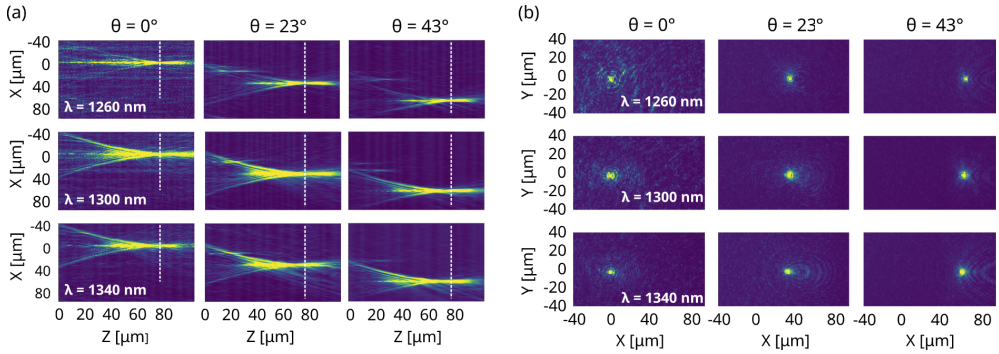

Fig. 4. Characterization in the 1300 nm wavelength range. Intensity profiles (a) in the axial xz plane and (b) at the image plane (transverse xy plane) for the same illuminating angles of Fig. 3 but with wavelength changing from 1260 nm to 1340 nm. The fix image plane marked by the white dashed line in (a) is located at z = 72 μm.

two ranges, respectively. This shift is approximately equal to the full width at half-maximum (FWHM) of the point spread function, measured as about 3.5 μm , which makes the behavior of the lens close to achromatic also in the transverse direction. Smaller deviations can be obviously obtained either reducing the bandwidth or the field of view of the lens.

The angular dependence of the FWHM of the point spread function is shown in Fig. 5(b). The average values across the two considered wavelength ranges are reported. As already mentioned, the quadratic phase profile introduces spherical aberration. As a result, the metalens does not reach the diffraction limit, which is reported for reference in the figure, and has a FWHM $\simeq 2\lambda$ (the measurements of the FWHM have an uncertainty of about 1 μm). This resolution is equivalent to that achieved by metalenses free of spherical aberration (such as the hyperbolic ones) with a numerical aperture of about 0.3. No significant differences can be observed between $\lambda = 1300$ nm and $\lambda = 1550$ nm and, importantly, the FWHM remains constant for increasing angle of incidence, which ensures the lens maintains good focusing properties also at tilted illumination. This is in marked contrast with hyperbolic metalenses that achieve diffraction-limited resolution

Optics EXPRESS

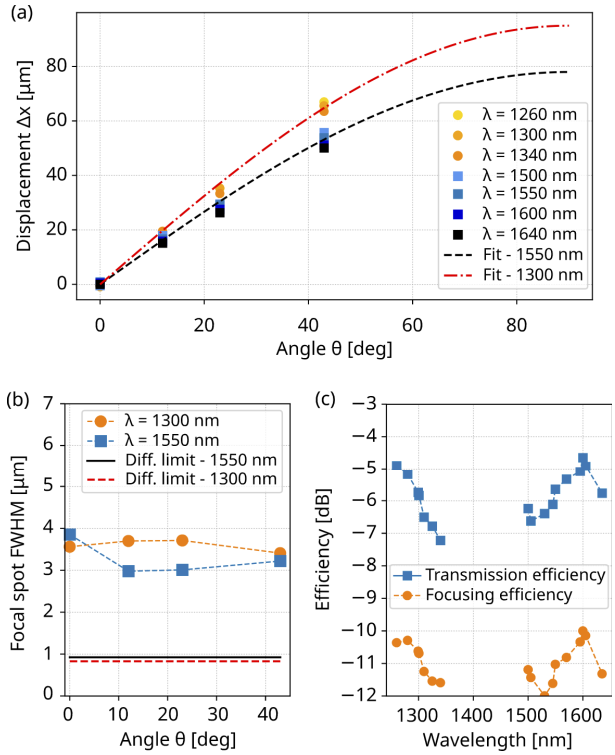

Fig. 5. Broadband performance of the metalens. (a) Displacement of the focal spot Δx in the x direction as a function of the incident angle θ for a few sampled wavelengths. Transverse chromatic aberration is smaller than the spot size within both wavelength ranges around 1300 nm and 1550 nm. (b) Average full width at half maximum of the focal spot in the two wavelength ranges as a function of θ. The diffraction limit is reported as well for reference. (c) Transmission and focusing efficiencies as a function of the wavelength. All measurements are done at fixed image planes for the two wavelength ranges.

but whose point spread function becomes heavily distorted even with small angles of incidence, making them unsuited for wide field of view operation.

Lastly, we quantified the wavelength dependence of the transmission and focusing efficiency of the lens, reported in Fig. 5(c) at normal incidence ($\theta = 0°$). The two efficiencies were determined by measuring the transmitted power in the area of the metalens and the transmitted power confined at the focal spot, respectively, normalized by the total power incident on the backside of the sample. Measurements were conducted at the same fixed image planes used in Fig. 3(b) and 4. The rather low transmission efficiency is mostly due to the reduced effective aperture of quadratic metalenses. At normal incidence, diffraction orders become evanescent at a distance from the lens axis larger than the focal distance (80 μm for the metalens considered here). Beyond this distance, light is mostly reflected and does not contribute to the focal spot, reducing the lens effective numerical aperture to about 0.71. It should also be noted, however, that with quadratic metalenses the field of view monotonically increases with the nominal numerical aperture and a value larger than 0.8 is still essential to achieve an arbitrarily large field of view [22,24]. Additional losses are introduced by the meta-atoms themselves, whose transmission efficiency was required to only be larger than 0.5 at normal incidence, as described in Sec. 2. The transmission of the meta-atoms is also non-uniform across the metalens which may cause a further degradation of the performance.

Optics EXPRESS

The difference between transmission and focusing efficiency can be explained by spherical aberration. It is interesting, however, how both transmission and focusing efficiencies exhibit a weak dependence on wavelength, with less than 2 dB fluctuations over the entire bandwidth between 1260 nm and 1640 nm. This is achieved despite the fact the meta-atoms used to realize the lens have been selected according to their transmission at λ = 1550 nm, as reported in Fig. 1(d). Additionally, the focusing efficiency of the lens with respect to the transmitted power fluctuates between 22% (-6.6 dB) and 36% (-4.4 dB) over the 380-nm bandwidth.

4. Conclusion

In summary, we have experimentally demonstrated that a single-layer metalens implementing a quadratic phase profile can simultaneously achieve a wide field of view and a broadband achromatic behavior. We realized a silicon-based metalens for the near-infrared and we characterized its performance at two wavelength ranges around λ = 1300 nm and λ = 1550 nm, respectively. Under tilted illumination, the focal spot of the lens remained free of off-axis aberrations and simply exhibited a transverse shift consistently throughout both spectral ranges, potentially reaching an arbitrarily large field of view. The FWHM of the focal spot remained almost constant at about 3.5 μm independently of the wavelength and illumination angle. Longitudinal chromatic aberration was limited to a 5% relative focal shift over a 140-nm bandwidth and was compensated by the relatively large depth of focus of the lens. The main limit to achromatic behavior was instead determined by transverse chromatic aberration which caused the position of the focal spot in the transverse direction for a given illumination angle to change with wavelength. However, even considering the largest possible field of view, transverse chromatic shift remained at most as large as the FWHM of the focal spot over the 140-nm bandwidth. Further extension of the operational bandwidth of the lens may be achieved by compensating for chromatic aberrations at design level. Beside the great potentialities as ultra-wide lenses for imaging applications [24], we believe the use of quadratic metalenses may prove particularly advantageous in the context of beam steering, for example in combination with focal plane switch arrays [27]. In this case, diffraction-limited resolution may not be required and the larger focal spot of quadratic metalenses does not represent a limitation for the performance of the system. On the contrary, their achromatic behavior and arbitrarily large field of view would offer an unprecedented route toward broadband photonic systems, paving the way to miniaturized devices for multispectral lidars [28] and free-space optical communications based on wavelength division multiplexing.

Funding. Agence Nationale de la Recherche (ANR-22-ERCS-0007-01); European Research Council.

Acknowledgments. The fabrication of the device was performed at the Plateforme de Micro-Nano-Technologie/C2N, which is partially funded by the Conseil General de l'Essonne. This work was partly supported by the French RENATECH network, by the Agence Nationale de la Recherche (ANR) under the Tremplin – ERC project ANR-22-ERCS-0007-01, and by the European Research Council (ERC) under the European Union's Horizon Europe research and innovation programme (project BEAMS, grant agreement No. 101041131).

Disclosures. The authors declare no conflicts of interest.

Data availability. All data generated or analyzed during this study may be obtained from the authors upon reasonable request.

Supplemental document. See Supplement 1 for supporting content.

References

1. P. Lalanne, S. Astilean, P. Chavel, E. Cambril, and H. Launois, "Design and fabrication of blazed binary diffractive elements with sampling periods smaller than the structural cutoff," J. Opt. Soc. Am. A **16**(5), 1143–1156 (1999).
2. N. Yu, P. Genevet, M. A. Kats, F. Aieta, J.-P. Tetienne, F. Capasso, and Z. Gaburro, "Light Propagation with Phase Discontinuities: Generalized Laws of Reflection and Refraction," Science **334**(6054), 333–337 (2011).
3. W.-J. Joo, J. Kyoung, M. Esfandyarpour, S.-H. Lee, H. Koo, S. Song, Y.-N. Kwon, S. H. Song, J. C. Bae, A. Jo, M.-J. Kwon, S. H. Han, S.-H. Kim, S. Hwang, and M. L. Brongersma, "Metasurface-driven OLED displays beyond 10, 000 pixels per inch," Science **370**(6515), 459–463 (2020).

Optics EXPRESS

4. S. M. Kamali, E. Arbabi, A. Arbabi, and A. Faraon, "A review of dielectric optical metasurfaces for wavefront control," Nanophotonics **7**(6), 1041–1068 (2018).
5. A. V. Kildishev, A. Boltasseva, and V. M. Shalaev, "Planar Photonics with Metasurfaces," Science **339**(6125), 1232009 (2013).
6. F. Aieta, P. Genevet, M. A. Kats, N. Yu, R. Blanchard, Z. Gaburro, and F. Capasso, "Aberration-Free Ultrathin Flat Lenses and Axicons at Telecom Wavelengths Based on Plasmonic Metasurfaces," Nano Lett. **12**(9), 4932–4936 (2012).
7. M. Khorasaninejad, W. T. Chen, R. C. Devlin, J. Oh, A. Y. Zhu, and F. Capasso, "Metalenses at visible wavelengths: Diffraction-limited focusing and subwavelength resolution imaging," Science **352**(6290), 1190–1194 (2016).
8. F. Presutti and F. Monticone, "Focusing on bandwidth: Achromatic metalens limits," Optica **7**(6), 624–631 (2020).
9. P. Lalanne and P. Chavel, "Metalenses at visible wavelengths: Past, present, perspectives," Laser Photonics Rev. **11**(3), 1600295 (2017).
10. H. Liang, A. Martins, B.-H. V. Borges, J. Zhou, E. R. Martins, J. Li, and T. F. Krauss, "High performance metalenses: Numerical aperture, aberrations, chromaticity, and trade-offs," Optica **6**(12), 1461–1470 (2019).
11. M. Khorasaninejad, Z. Shi, A. Y. Zhu, W. T. Chen, V. Sanjeev, A. Zaidi, and F. Capasso, "Achromatic Metalens over 60 nm Bandwidth in the Visible and Metalens with Reverse Chromatic Dispersion," Nano Lett. **17**(3), 1819–1824 (2017).
12. E. Arbabi, A. Arbabi, S. M. Kamali, Y. Horie, and A. Faraon, "Controlling the sign of chromatic dispersion in diffractive optics with dielectric metasurfaces," Optica **4**(6), 625–632 (2017).
13. S. Shrestha, A. C. Overvig, M. Lu, A. Stein, and N. Yu, "Broadband achromatic dielectric metalenses," Light: Sci. Appl. **7**(1), 85 (2018).
14. S. Wang, P. C. Wu, V.-C. Su, Y.-C. Lai, M.-K. Chen, H. Y. Kuo, B. H. Chen, Y. H. Chen, T.-T. Huang, J.-H. Wang, R.-M. Lin, C.-H. Kuan, T. Li, Z. Wang, S. Zhu, and D. P. Tsai, "A broadband achromatic metalens in the visible," Nat. Nanotech. **13**(3), 227–232 (2018).
15. A. Ndao, L. Hsu, J. Ha, J.-H. Park, C. Chang-Hasnain, and B. Kanté, "Octave bandwidth photonic fishnet-achromatic-metalens," Nat. Commun. **11**(1), 3205 (2020).
16. A. Arbabi, E. Arbabi, S. M. Kamali, Y. Horie, S. Han, and A. Faraon, "Miniature optical planar camera based on a wide-angle metasurface doublet corrected for monochromatic aberrations," Nat. Commun. **7**(1), 13682 (2016).
17. B. Groever, W. T. Chen, and F. Capasso, "Meta-Lens Doublet in the Visible Region," Nano Lett. **17**(8), 4902–4907 (2017).
18. M. Y. Shalaginov, S. An, F. Yang, P. Su, D. Lyzwa, A. M. Agarwal, H. Zhang, J. Hu, and T. Gu, "Single-Element Diffraction-Limited Fisheye Metalens," Nano Lett. **20**(10), 7429–7437 (2020).
19. J. Engelberg, C. Zhou, N. Mazurski, J. Bar-David, A. Kristensen, and U. Levy, "Near-IR wide-field-of-view Huygens metalens for outdoor imaging applications," Nanophotonics **9**(2), 361–370 (2020).
20. F. Yang, S. An, M. Y. Shalaginov, H. Zhang, C. Rivero-Baleine, J. Hu, and T. Gu, "Design of broadband and wide-field-of-view metalenses," Opt. Lett. **46**(22), 5735–5738 (2021).
21. Z. Huang, M. Qin, X. Guo, C. Yang, and S. Li, "Achromatic and wide-field metalens in the visible region," Opt. Express **29**(9), 13542–13551 (2021).
22. M. Pu, X. Li, Y. Guo, X. Ma, and X. Luo, "Nanoapertures with ordered rotations: Symmetry transformation and wide-angle flat lensing," Opt. Express **25**(25), 31471–31477 (2017).
23. Y. Guo, X. Ma, M. Pu, X. Li, Z. Zhao, and X. Luo, "High-Efficiency and Wide-Angle Beam Steering Based on Catenary Optical Fields in Ultrathin Metalens," Adv. Opt. Mater. **6**(19), 1800592 (2018).
24. A. Martins, K. Li, J. Li, H. Liang, D. Conteduca, B.-H. V. Borges, T. F. Krauss, and E. R. Martins, "On Metalenses with Arbitrarily Wide Field of View," ACS Photonics **7**(8), 2073–2079 (2020).
25. E. Lassalle, T. W. W. Mass, D. Eschimese, A. V. Baranikov, E. Khaidarov, S. Li, R. Paniagua-Dominguez, and A. I. Kuznetsov, "Imaging Properties of Large Field-of-View Quadratic Metalenses and Their Applications to Fingerprint Detection," ACS Photonics **8**(5), 1457–1468 (2021).
26. J. P. Hugonin and P. Lalanne, "Reticolo software for grating analysis," arXiv preprint arXiv:2101.00901 (2021).
27. C. Rogers, A. Y. Piggott, D. J. Thomson, R. F. Wiser, I. E. Opris, S. A. Fortune, A. J. Compston, A. Gondarenko, F. Meng, X. Chen, G. T. Reed, and R. Nicolaescu, "A universal 3D imaging sensor on a silicon photonics platform," Nature **590**(7845), 256–261 (2021).
28. N. Li, C. P. Ho, I.-T. Wang, P. Pitchappa, Y. H. Fu, Y. Zhu, and L. Y. T. Lee, "Spectral imaging and spectral LIDAR systems: Moving toward compact nanophotonics-based sensing," Nanophotonics **10**(5), 1437–1467 (2021).